Talanta 182 (2018) 116–124

Contents lists available at ScienceDirect

Talanta

journal homepage: www.elsevier.com/locate/talanta

A turn-on chemiluminescence biosensor for selective and sensitive detection of adenosine based on HKUST-1 and QDs-luminol-aptamer conjugates

Yanna Lin, Yuxue Dai, Yuanling Sun, Chaofan Ding, Weiyan Sun, Xiaodong Zhu, Hao Liu, Chuannan Luo*

Key Laboratory of Interfacial Reaction & Sensing Analysis in Universities of Shandong, School of Chemistry and Chemical Engineering, University of Jinan, Jinan 250022, PR China

ARTICLE INFO

Keywords:
CdTe QDs-luminol-aptamer
Chemiluminescence
HKUST-1
Catalyst
Adenosine

ABSTRACT

In this work, HKUST-1 and QDs-luminol-aptamer conjugates were prepared. The QDs-luminol-aptamer conjugates can be adsorbed by graphene oxide through π-π conjugation. When the adenosine was added, the QDs-luminol-aptamer conjugates were released from magnetic graphene oxide (MGO), the chemiluminescent switch was turned on. It was reported that HKUST-1 can catalyze the chemiluminescence reaction of luminol-H_2O_2 system in an alkaline medium, and improve the chemiluminescence resonance energy transfer (CRET) between chemiluminescence and QDs indirectly. Thus, the adenosine can be detected sensitively. Based on this phenomenon, the excellent platform for detection of adenosine was established. Under the optimized conditions, the linear detection range for adenosine was 1.0×10^{-12}–2.2×10^{-10} mol/L with a detection limit of 2.1×10^{-13} mol/L. The proposed method was successfully used for adenosine detection in biological samples.

1. Introduction

Chemical sensors are commonly used in environmental pollution monitoring [1–5], medical diagnosis [6], biological work [7–9] and other fields. According to the different test objects, chemical sensors can be divided into gas sensors [10], humidity sensors [11], ion sensors [12–15] and biosensors [16,17]. Currently used detection methods are electrochemical, fluorescence, chemiluminescence and surface enhanced Raman spectroscopy. Due to its high sensitivity, simple instruments and wide linearity, chemiluminescence (CL) has been proved to be a powerful technique for trace detection of analytes [18,19]. There are a number of chemiluminescent systems, in which luminol-H_2O_2 is more commonly used. Chemiluminescence resonance energy transfer (CRET) is non-radiative energy transfer from a chemiluminescent donor to an energy acceptor. The conventional CRET was rarely applied to analysis, due to its poor transfer efficiency and a few number of energy acceptors. The introduction of nanomaterials, such as QDs, gold nanoparticles and graphene [20], can effectively improve the inherent drawbacks of CRET.

QDs has large Stokes shifts and high luminescence efficiency, and it is excellent energy acceptor. Due to these merits of QDs, it has been widely used in food [21], disease [22,23] and heavy metal [24] testing. Lin et al. [25] had compared the CL intensity of CdTe quantum dots, CdS quantum dots, and CdSe quantum dots, and they found that CdTe QDs could greatly enhance the CL intensity than that of CdS and CdSe QDs at the same concentration. However, it has been reported that H_2O_2 could oxidize QDs and quench the luminescence [26]. Thus, preventing the oxidation of QDs is particularly important for bioanalysis. Wang et al. [27] synthesized luminol-QDs conjugates for the first time, and they confirmed that an efficient CRET occurred in luminol-QDs conjugates. Duan et al. [28] utilized the QDs@luminol conjugates to construct a sensor for the detection of chrysoidine based on CRET.

Metal-organic frameworks (MOFs) are composed of metal ions or metal clusters and organic ligands. Due to its large surface areas, tunable cavities, controlled pore sizes, and catalysis activity, MOFs have received increasing attention in the fields of gas storage, catalysis, drug delivery and sensing. The group of Dirk E. De Vos [29] observed the well-defined Lewis acid sites and the high selectivities of HKUST-1 for several important isomerization reactions, which are strong incentive for the exploration of MOF as catalysts. In the field of analytical chemistry, the application of MOFs is evolving, especially in biosensors. Luo et al. [30] synthesized a solid catalyst by encapsulating Hemin into the HKUST-1 MOF materials, and constructed a sensor for the detection of H_2O_2 and glucose. They obtained a satisfactory result and shown that the solid catalyst has strong catalytic activity for chemiluminescence. The team of Chen [31] used the catalytic effect of HKUST-1 to construct a sensor for the detection of dopamine, and obtained a satisfactory result. Besides, some other MOFs materials in the biosensor applications

* Corresponding author.
E-mail address: chm_yfl518@163.com (C. Luo).

https://doi.org/10.1016/j.talanta.2018.01.065
Received 26 October 2017; Received in revised form 24 January 2018; Accepted 29 January 2018
Available online 31 January 2018

are also more and more widely [32–37].

The graphene oxide (GO) is mainly composed of carbon atoms in the form of sp^2 hybridized by covalent bonding, having a two-dimensional lamellar structure and a large specific surface area. GO has been widely used in different research areas, such as electronic devices [38], optical communication [39], solar cells [40–42], lithium ion batteries [43,44], DNA sequencing [45], sensors [46,47], supercapacitors [48,49] and adsorbent materials [50]. Since the graphene-based plane has a unoxidized conjugated benzene ring structure, protein and aptamer can be adsorbed on the surface of GO by π-π interaction and electrostatic interaction. Combined with the nature of magnetic graphene oxide (MGO) easy to separate, GO is an important material for building biosensors.

Adenosine is an endogenous nucleoside, and it has physiological effects on the cardiovascular system and other tissues of the body. The study found that the rapid growth of tumors can lead to the degradation of adenine nucleotide and release adenosine, which is highly expressed in tumors [51]. Thus, adenosine can be used as a tumor marker to investigate the development degree of tumor. Sensitive detection of adenosine is of great significance in the diagnosis of clinical diseases. At present, hybridization chain reaction [52], electrochemistry [53,54], fluorescence [55], chemiluminescence [56], and colorimetry [57] have been widely used in the detection of adenosine, the detection limit of these methods range from 3.2×10^{-11} to 4.2×10^{-7} mol/L. In addition, the biological enzyme as a signal amplification factor is also increasingly widely used in the construction of the sensor [53,58,59]. However, the biological enzyme is sensitive to the environment, its activity and stability are difficult to control. Therefore, a new sensitive enzyme-free method for the detection of adenosine is essential.

Herein, coupling with peroxidase activity of HKUST-1 and CRET of QDs-luminol-aptamer conjugates, a magnetic separate "turn-on" chemiluminescence biosensor based on MGO was designed for adenosine detection (Scheme 1). The catalyst was prepared using 1,3,5-benzenetricarboxylic acid as ligand and $Cu(NO_3)_2$ as metal node. Luminol was immobilized on the QDs to improve CRET and prevent QDs from agglomerating and being oxidized. Due to the π-π interaction between aptamer and MGO, the adenosine aptamers were also modified on the surface of QDs to build chemiluminescent switch. In the absence of adenosine, QDs-luminol-aptamer conjugates were adsorbed on MGO, no chemiluminescence signal was detected. When the adenosine was added, the conjugates fell off MGO and the chemiluminescent switch was turned on. For the first time, we combined HKUST-1 with QDs-luminol-aptamer conjugates and used them for the chemiluminescence analysis of adenosine. The resulting QDs-luminol-aptamer composites limit luminol to the surface of QDs, which shortens the distance between the energy donor and the acceptor and improves the CRET efficiency. The ability of aptamers to specifically recognize targets improves the selectivity of the system. The introduction of HKUST-1 accelerates the decomposition of H_2O_2, promotes the chemiluminescence reaction between luminol and H_2O_2, improves the signal to noise ratio, and further improves CRET indirectly. The HKUST-1-based sensor with enhanced light intensity was easily used to detect adenosine with a detection limit of 2.1×10^{-13} mol/L, and shown a great potential in complex samples. The HKUST-1-based strategy has great potential application in signal amplification and monitoring the important biomolecules in the biological system.

2. Experimental section

2.1. Reagents and materials

Cadmium chloride ($CdCl_2$), Sodium thioglycolate (80%), $NaBH_4$ (96%), 1-(3-dimethylaminopropyl)-3-ethylcarbodiimide hydrochloride (EDC, 95%) and anhydrous ethanol were purchased from Sinopharm Group Reagent Co., Ltd. (Shanghai, China). Copper nitrate trihydrate ($Cu(NO_3)_2$) was obtained from Tianjin Pepsi Chemical Co., Ltd. (Tianjin, China). Tellurium (Te, 99%), 1,3,5-benzenetricarboxylic acid (H_3BTC, 98%) were purchased from Shanghai Jing chun biochemical Technology Co., Ltd. (Shanghai, China). Methanol, N, N-dimethyl formamide (DMF) were obtained from Tianjin Fuyu Fine Chemical Co., Ltd. (China). N-Hydroxysuccinimide (NHS) was obtained from Shanghai Civi Chemical Technology Co., Ltd. (Shanghai, China). Luminol was purchased from Xiya Co. Ltd. Adenosine purchased from Macklin Biochemical Technology Co., Ltd. (Shanghai, China). Superoxide dismutase and adenosine aptamer were obtained from Sangon Biotechnology Co. Ltd. (Shanghai, China). The sequences of the aptamer is 5′-NH_2-AGA GAA CCT GGG GGA GTA TTG CGG AGG AAG GTT −3′.

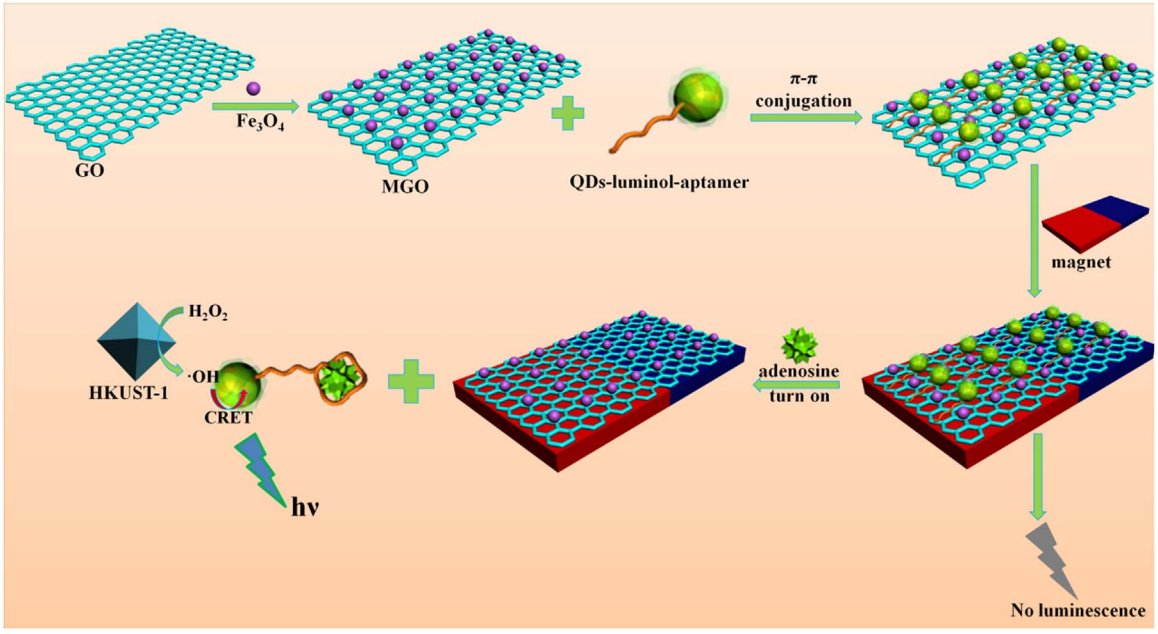

Scheme 1. Schematic illustration of CL sensor based on the catalytic effect of HKUST-1.

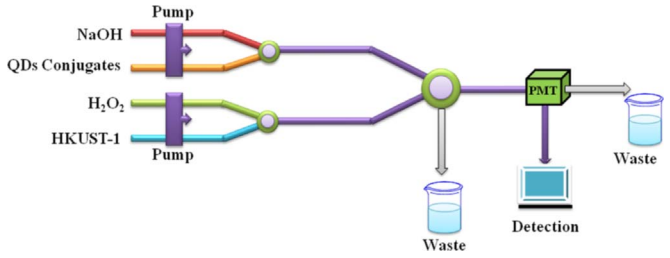

Fig. 1. The schematic diagram of the CL sensor.

2.2. Apparatus

Scanning electron microscope (SEM) images were obtained from a JEM-2100 microscope (JEOL, Japan). Transmission electron microscopic (TEM) image was obtained from a JEOL1400 microscope (Japan). X-ray diffraction (XRD) patterns were obtained from D8 focus diffractometer (Bruker AXS, Germany). UV–vis absorption spectra were obtained from a Lambda 35 UV–vis spectrometer (PerkinAElmer, USA). Fourier transforminfrared spectroscopy (FTIR) analyses were recorded on a PerkinElmer spectrometer (PerkinAElmer, USA) using KBr pellets. Fluorescence experiments were carried out on a Shimadzu Fluorescence Spectrophotometer (RF-5301, Japan). Nitrogen adsorption and desorption experiment was carried out with a specific surface area and pore size analyzer (TristarII, China). All chemiluminescence experiments were carried out using a IFFM-E flow injection CL analyzer (Xi'an Remex Electronic instrument High-Tech Ltd., China). The schematic diagram of the CL sensor used in this work was shown in Fig. 1.

2.3. Synthesis of GO and MGO

The GO was synthesized from natural graphite powders by a modified Hummers method [60]. Firstly, 1 g graphite powder was placed into a 500 mL of flask, and 200 mL of mixed acid was added into the flask. After stirring 0.5 h, $KMnO_4$ (6 g) was added into the flask and stirring for another 1 h. Then, the mixture was heated in an oil bath at 90 °C for 12 h. Next, under the condition of the ice bath, slowly added H_2O_2 until no more reaction. The mixture was centrifuged and the resulting precipitates were washed several times with 30 mL 0.2 mol/L HCl and ethanol, respectively. After vacuum drying, the resulting brownish sample was GO.

MGO was prepared according to the method of Kassaee' group [61]. 0.2 g of GO was scattered in 30 mL H_2O and ultrasound dispersion for 0.5 h. $FeCl_3$ (0.2 g) and $FeCl_2$ (0.14 g) were added into the disperse GO solution, and the value of pH was adjusted to 9.0 with $NH_3{\cdot}H_2O$ under the protection of N_2. Next, the diluted suspension was stirred at 90 °C and refluxed for 0.5 h. The precipitates were isolated in the magnetic field and washed with 150 mL of ethanol. Finally, the products were air-dried.

2.4. Synthesis of QDs-luminol-aptamer conjugates

The preparation of QDs was performed according to a previous method with some modifications [25]. In this work, 0.03975 g Te and 0.0540 g $NaBH_4$ were dissolved in 15 mL of H_2O stirring for 1 h under the protection of N_2, the resulting solution was called solution A; 0.1142 g $CdCl_2$ and 0.1377 g sodium thioglycolate were dissolved in 300 mL H_2O and the pH of the resulting solution was adjusted to 11.2 with NaOH, stirring for 0.5 h under the protection of N_2, the resulting solution was called solution B. The solution A was mixed with solution B and the precursors were converted to CdTe nanocrystals by refluxing the reaction mixture at 100 °C for 13.5 h. The resulting products were washed with methanol and dried in a vacuum oven to obtain a brown powder.

The QDs-luminol-aptamer conjugates were synthesized according to the previous literature with some modification [27]. 0.05 g of QDs were dispersed in the phosphate buffer solution (pH 7.4) and then EDC and NHS were added into the QDs suspension to activate the QDs. Next, luminol were added into the mixture to gain the QDs-luminol conjugates. The preparation process of QDs-luminol-aptamer conjugates was exactly the same as that for the preparation of corresponding QDs-luminol unless aptamers were added into the solution.

2.5. The synthesis of HKUST-1

HKUST-1 was synthesized according to the previous literature [62]. 0.8750 g of $Cu(NO_3)_2{\cdot}3H_2O$ was dissolved in 12 mL of H_2O and 0.4200 g of H_3BTC was dissolved in 12 mL of ethanol. Then the solution were mixed before it was placed in a 50 mL Teflon-lined autoclave and maintained at 120 °C for 12 h under static condition. After slowly cooling to room temperature, the blue precipitates were separated from the reaction mixture by centrifuge and rinsed thoroughly with abundance of DMF and deionized water. The resulting products were dried in a vacuum oven.

2.6. Adsorption performance of MGO

The adsorption properties of MGO on QDs-luminol-aptamer conjugates were studied in this work. 1 mg of MGO was placed into 25 mL tubes. Next, different volume doses of 0.5 mg/mL of QDs-luminol-aptamer conjugates were added to the tubes, respectively. The tubes were shaken at room temperature for 1 h. Under the action of magnetic field, the supernatant of the tubes were detected by a CL instrument and the adsorption capacities were calculated.

1 mg of MGO was dispersed in 13 mL QDs-luminol-aptamer conjugates, and shook for 0.5 min, 1 min, 3 min, 5 min, 10 min, 15 min, 18 min, and 20 min, respectively. Under the action of magnetic field, the supernatant of the tube was detected by CL instrument and the adsorption capacities were calculated.

The adsorption capacities were calculated from the following formula:

$$Q = \frac{(c_0 - c_e)V}{m}$$

Where Q (μg/mg) was the mass of QDs-luminol-aptamer conjugates adsorbed by unit mass of dry MGO, c_0 (μg/mL) and c_e (μg/mL) were the concentration of QDs-luminol-aptamer conjugates in the initial and final solution, respectively. V (mL) was the volume of the adsorption mixture, and m (mg) was the mass of the MGO.

3. Results and discussion

3.1. Concept of the design

In this work, a simple, rapid, and sensitive CL sensing strategy based on the peroxidase-like catalytic activity of HKUST-1 is reported. This strategy relies on the fact that the adenosine could bind specifically to the aptamer and cause the QDs-luminol-aptamer conjugates fell off the MGO. Thus, the CL switch is turned on, as shown in Scheme 1. The CRET efficiency can be defined in the equation $E = 1/(1+\frac{R^6}{R_0^6})$, where R_0 is the distance leading to 50% of energy transfer from the donor to the acceptor, R is the distance between donor and acceptor. In order to shorten the distance between donor and acceptor, QDs-luminol-aptamer conjugates were used to construct a CL method for adenosine detection.

3.2. Characterizations of GO and MGO

SEM, FTIR and XRD were used to elucidate the morphology of GO and MGO. As shown in Fig. 2(A), the thickness of GO is fold of thin

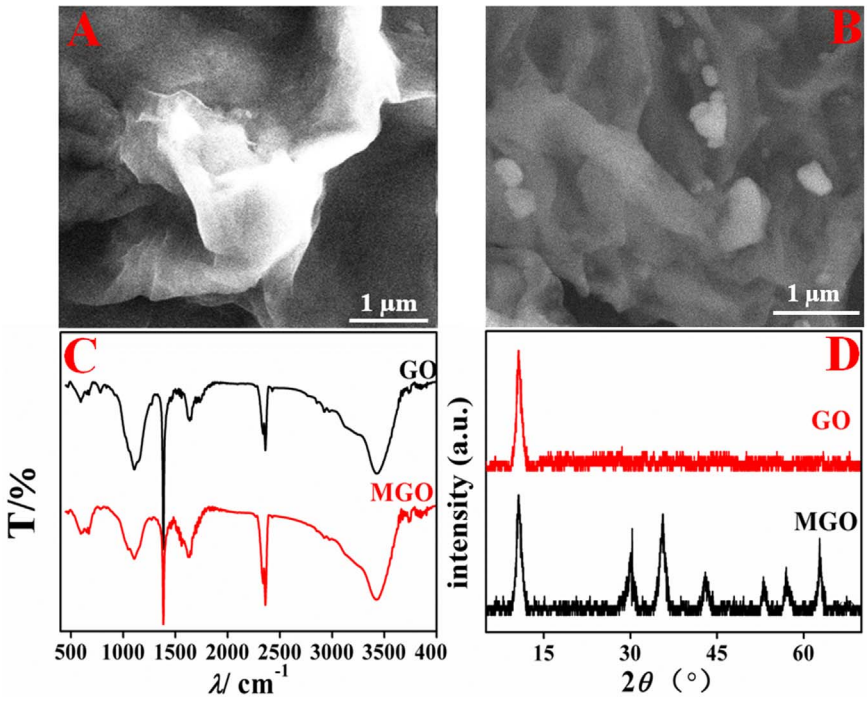

Fig. 2. (A) SEM of GO, (B) SEM of MGO, (C)FTIR of GO and MGO and (D) XRD of GO and MGO.

monolayer structure and the surface if rough, which increased the surface area. While the surface of MGO (Fig. 2B) is multi-layer, the surface is rugged and coated by Fe_3O_4. The chemical groups on the surface of GO and MGO were investigated by FTIR spectra, as shown in Fig. 2(D). 1401 cm^{-1} and 1643 cm^{-1} are the characteristics of benzene ring, the adsorption peak at 1062 cm^{-1} indicates the C-O group's stretching vibration. As shown, the peak at 621 cm^{-1} is the characteristic of Fe_3O_4. What's more, there is a narrow and relatively strong diffraction peak at about $2\theta = 10^{\circ}$ that is the characteristic peak of GO in the XRD patterns (Fig. 2D). Besides, the diffraction peak at $2\theta =$ 30.2°, 35.5°, 43.2°, 53.6°, 57.1° and 62.7° are the characteristic peaks of Fe_3O_4 in the Fig. 2(D). All characterizations are indicative of the successful synthesis of GO and MGO.

3.3. Characterizations of QDs and QDs-luminol-aptamer conjugates

TEM was used to elucidate the size and morphology of the QDs. As shown in Fig. 3(A), the QDs have a uniform spherical structure and the average particle size is about 8 nm. Fig. 3 (B) shows the FTIR spectra of QDs, QDs-luminol and luminol respectively. It could be seen that

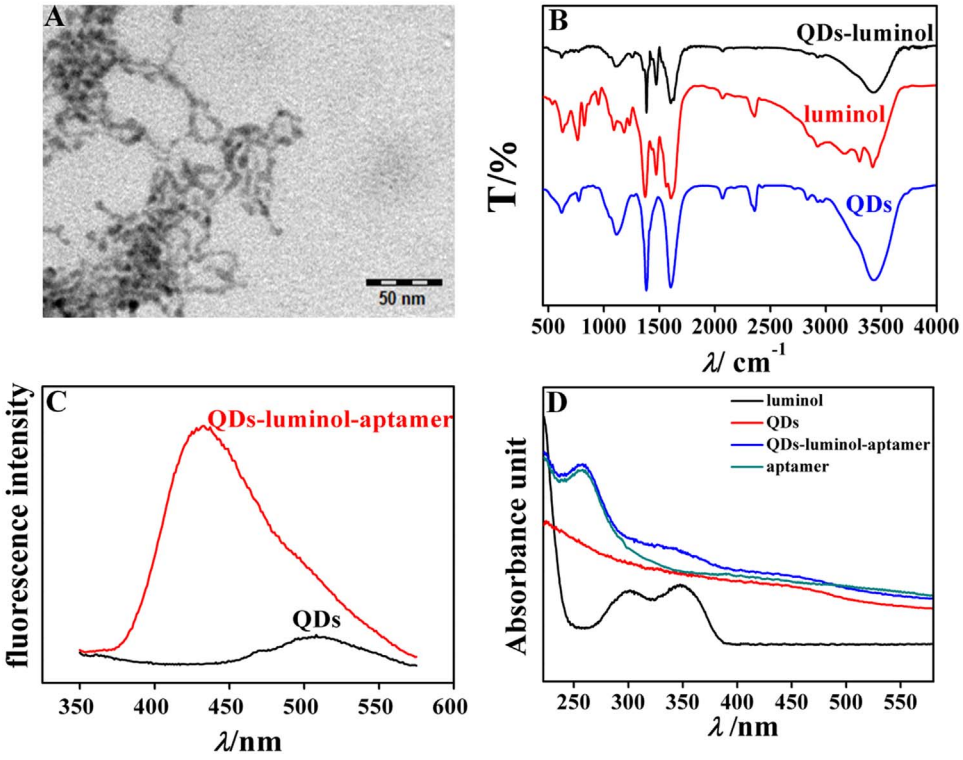

Fig. 3. (A) The TEM of QDs. (B) FTIR of QDs, QDs-luminol and QDs-luminol-aptamer. (C) Fluorescence spectroscopy of QDs and QDs-luminol-aptamer. (D) UV spectrum of QDs, QDs-luminol-aptamer, aptamer and luminol.

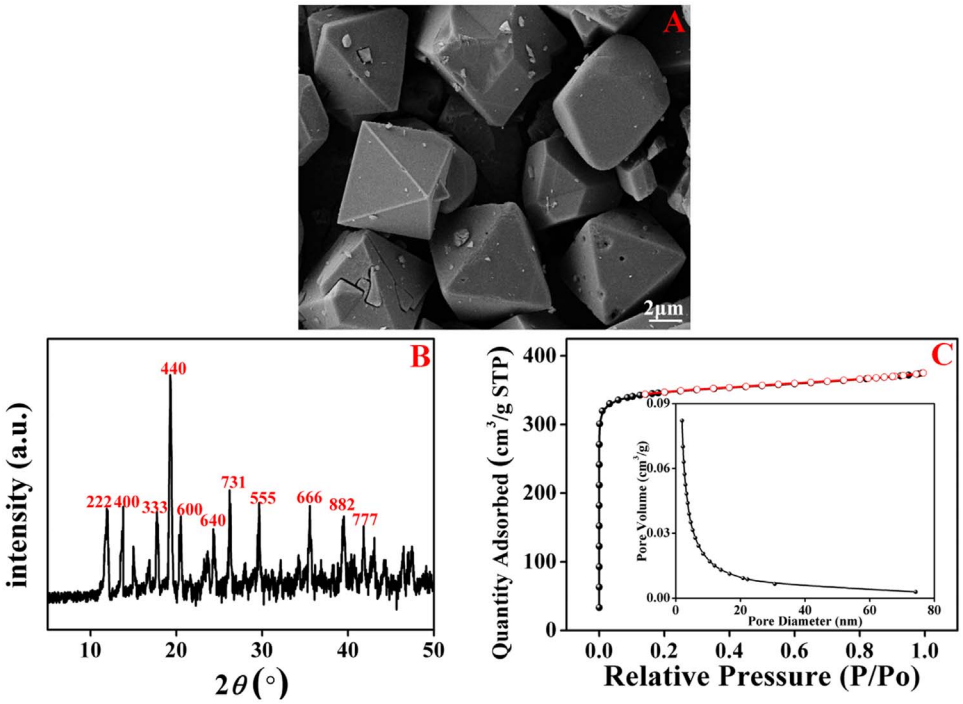

Fig. 4. SEM (A), XRD (B) and BET (C) of HKUST-1.

symmetrical stretching vibration of C-S bond contributes to the strong absorption at 1200 cm^{-1}. The peak at 1255 cm^{-1} is the result of the stretching vibration of C-N in the secondary amide. 1380 cm^{-1} and 1475 cm^{-1} are the bending vibration absorption peak of C-H and C-N, respectively. The peak at 1560 cm^{-1} is the bending vibration absorption peak of N-H bond in the amide. The peak at 1580 cm^{-1} is the result of asymmetric stretching vibration of C=O bond. There is a broad and strong absorption peak at 3500 cm^{-1}, which is the absorption peak of -OH.

As seen, the fluorescence intensity of QDs-luminol-aptamer complex is stronger than that of QDs with the blue shift of the maximum emission in Fig. 3 (C). What's more, both QDs-luminol-aptamer and QDs solution contained 0.8 mol/L of H_2O_2. The O_2 produced by decomposition of H_2O_2 occupied the electron-hole defects on the surface of QDs. At this point, QDs became good electron acceptors, forming non-fluorescent QDs anions and leading to fluorescence quenching. Under the effect of EDC/NHS, the carboxyl groups on the surface of the QDs were covalently bonded to the amino group of luminol and aptamers, and the number of charge on the surface of QDs is reduced, which reduces the directional polarization around the QDs. The reduction of directional polarization causes the decrease of Stokes shift. Therefore, the maximum emission of QDs-luminol-aptamer is blue shifted.

The UV–vis absorption of QDs, QDs-luminol-aptamer conjugates, aptamer and luminol is shown in Fig. 3 (D), QDs have the highest UV absorption at 476 nm and UV absorption of luminol is 348 nm. Aptamers have the highest UV absorption at 258 nm. It is worth noting that the QDs-luminol-aptamer has both the UV absorption characteristics of luminol, aptamer and the ultraviolet absorption characteristics of QDs, which indicates the QDs-luminol-aptamer composites were synthesized successfully.

3.4. Characterizations of HKUST-1

SEM image clearly shows the octahedral structure of HKUST-1 with the average diameter less than 10 μm (Fig. 4A). As shown in Fig. 4(B), the diffraction peak at 2θ = 11.6°, 13.4°, 17.4°, 19°, 20.2°, 24.3°, 25.9°, 35.3°, 39.2° and 41.5° correspond to the (222), (400), (333), (440), (600), (640), (731), (555), (666), (882) and (777) crystal surface of HKUST-1, respectively. The XRD data of HKUST-1 indicates that HKUST-1 has a good crystal structure. The Brunauer-Emmett-Teller (BET) isotherm experimental results (Fig. 4C) suggest that HKUST-1 exhibits typical type-I isotherm characteristics of microporous materials. The BET surface areas of HKUST-1 was measured to be 1049.8 m^2/g, which laid the foundation for its catalysis.

3.5. Catalytic activity of HKUST-1

In alkaline solution (e.g., 0.1 mol/L NaOH), the catalytic activity of HKUST-1 for the CL reaction between luminol and H_2O_2 was investigated. The CL spectra of luminol-NaOH-HKUST-1, luminol-NaOH-H_2O_2, luminol-NaOH-H_2O_2-HKUST-1, luminol-NaOH-QDs-H_2O_2-HKUST-1, QDs-luminol-aptamer complex-NaOH-H_2O_2-HKUST-1 systems were presented in Fig. 5. As shown in Fig. 5(a), no CL was found for luminol-NaOH-HKUST-1 system. In contrast, luminol-NaOH-H_2O_2 and luminol-NaOH-H_2O_2-HKUST-1 systems exhibit strong CL. What's more, the CL intensity of luminol-NaOH-H_2O_2-HKUST-1 is stronger than luminol-NaOH-H_2O_2, which shows that the HKUST-1 has a catalytic effect on the luminol-H_2O_2 system. However, the CL intensity of luminol-NaOH-QDs-H_2O_2-HKUST-1 system is stronger than the CL intensity of luminol-NaOH-H_2O_2-HKUST-1, which indicates that the

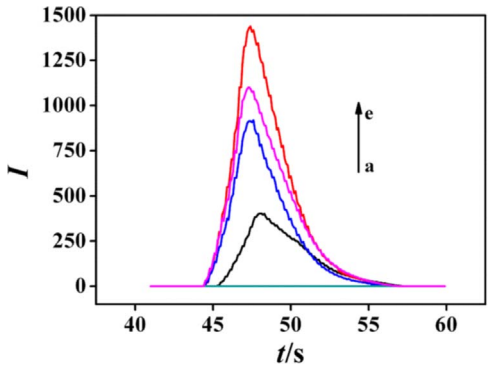

Fig. 5. The CL spectra of different CL systems. (a) luminol-NaOH-HKUST-1; (b) luminol-NaOH-H_2O_2; (c) luminol-NaOH-H_2O_2-HKUST-1; (d) luminol-NaOH-QDs-H_2O_2-HKUST-1; (e) QDs-luminol-aptamer complex-NaOH-H_2O_2-HKUST-1.

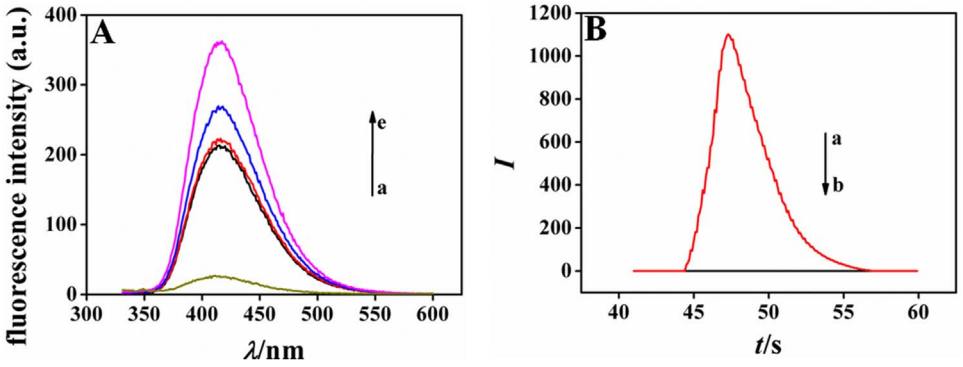

Fig. 6. (A) The effect of HKUST-1 concentration on·OH formation with terephthalic acid as a fluorescence probe. (a) $C_{HKUST-1}$, 0 mg/L; (b) $C_{HKUST-1}$, 5 mg/L; (c) $C_{HKUST-1}$, 10 mg/L; (d) $C_{HKUST-1}$, 20 mg/L; (e) $C_{HKUST-1}$, 30 mg/L. (B) CL spectra of luminol in the absence (a) and presence (b) of superoxide dismutase.

CRET caused by the addition of QDs can also enhance the intensity of CL. But QDs can be oxidized by H_2O_2. Thus, the problem of oxidizing the QDs by H_2O_2 was solved in the work. The QDs-luminol-aptamer complex-NaOH-H_2O_2-HKUST-1 system was constructed and its CL spectra was measured in Fig. 5(e). As seen in Fig. 5, the CL intensity of QDs-luminol-aptamer complex-NaOH-H_2O_2-HKUST-1 system is highest. There are two possible reasons: on the one hand, the luminol modified on the surface of QDs, which can effectively avoid the oxidation of H_2O_2 and the CL reaction was confined on the surface of QDs accordingly, thereby improving CRET efficiency; on the other hand, HKUST-1 could promote the decomposition of H_2O_2 to catalyze CL reaction and improve CRET indirectly.

Based on the HKUST-1 catalysis, we believe that the possible mechanisms are as follows:

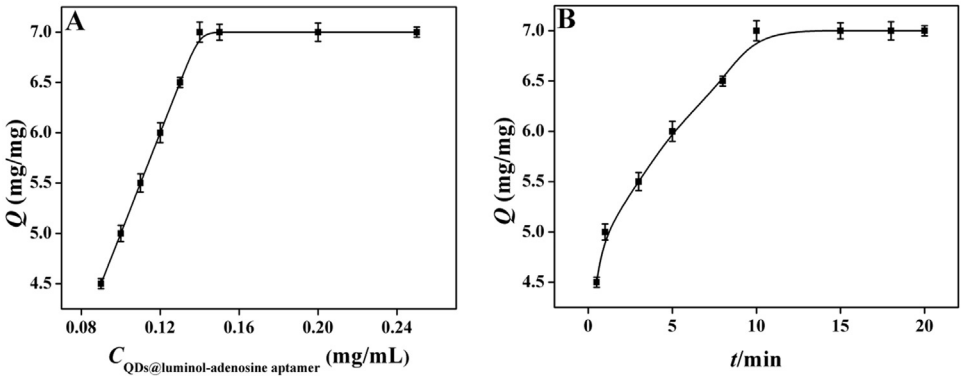

Fig. 7. The adsorption properties of MGO.

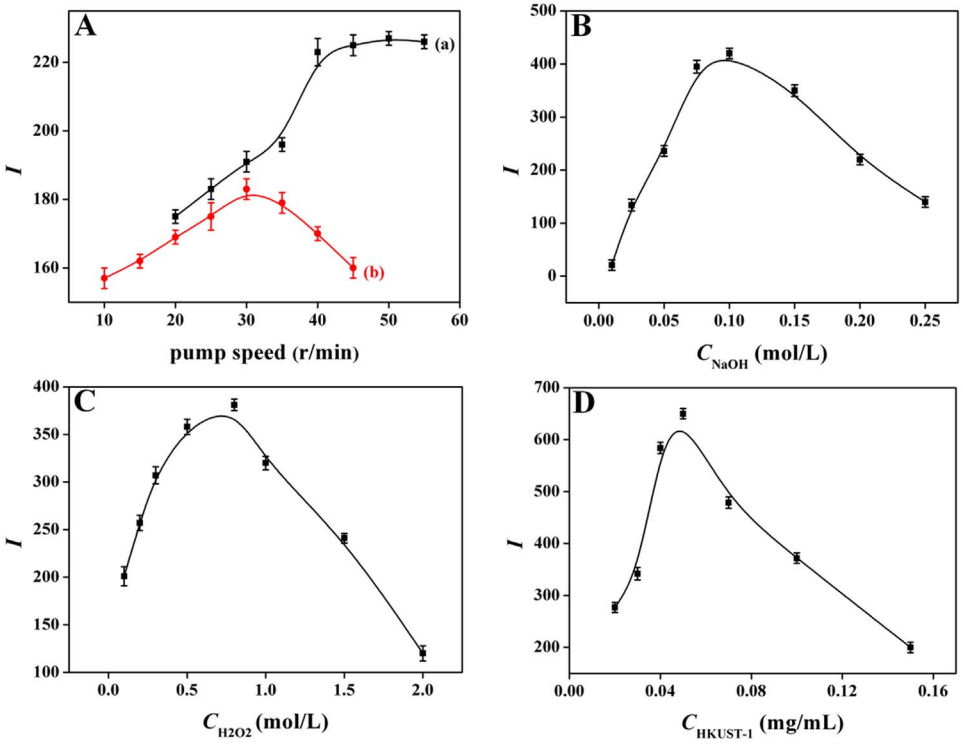

Fig. 8. (A) The optimization of pump speed, (a) vice pump, (b) main pump; (B) The optimization of NaOH concentration; (C) The optimization of H_2O_2 concentration; (D) The optimization of H_2O_2 concentration.

Firstly, the transition metal can catalyze the decomposition of H_2O_2, and HKUST-1 contains Cu^{2+}. The catalytic process is expressed by the formula (1, 2, 3).

$$H_2O_2 + Cu^{2+} \rightarrow Cu^{3+} + \bullet OH + OH^- \quad (1)$$

$$H_2O_2 + Cu^{3+} \rightarrow Cu^{2+} + \bullet OOH + H^+ \quad (2)$$

$$\bullet OOH + Cu^{3+} \rightarrow Cu^{2+} + \bullet O_2^- + H^+ \quad (3)$$

The activation energy of these reactions are low, and the reaction rate is very fast at room temperature.

Second, the catalytic activity of HKUST-1 is not only related to the Cu^{2+} active site but also to the micropores and the high specific surface area of HKUST-1. High specific surface area and electronic strength make further improvement in catalytic activity of HKUST-1. What's more, HKUST-1 is capable of activating H_2O_2 by local electron exchange to produce •OH [31]. Therefore, HKUST-1 is able to catalyze CL reaction between luminol and H_2O_2 to enhance CL.

To verify the above speculations, we demonstrated the presence of •OH and $\bullet O_2^-$, respectively, using terephthalic acid and superoxide dismutase, as shown in Fig. 6. The fluorescence intensity was weak in the absence of HKUST-1 and gradually increased as the concentration of HKUST-1 increased (Fig. 6A), indicating that HKUST-1 promoted the formation of •OH by H_2O_2 decomposition. CL spectras of luminol in the absence and presence of superoxide dismutase are presented in Fig. 6(B). After addition of superoxide dismutase, chemiluminescence was quenched, indicating that $\bullet O_2^-$ was generated and played an important role in chemiluminescence reactions.

Finally, the synthesis of the QDs-luminol complex effectively protected the QDs from being oxidized and the CL reaction was carried out on the surface of the QDs, improving the CRET efficiency and further improving the sensitivity of the method.

3.6. Adsorption properties of MGO

The adsorption performance of MGO for QDs-luminol-aptamer was measured and shown in Fig. 7. The adsorption capacities for QDs-luminol-aptamer at different initial concentrations are shown in Fig. 7 (A). The adsorption capacity for QDs-luminol-aptamer increased with increasing QDs-luminol-aptamer concentration before reaching a maximum of 7 mg/mg. Fig. 7 (B) showed the adsorption kinetics of MGO for QDs-luminol-aptamer. QDs-luminol-aptamer conjugates could reach maximum adsorption within 10 min.

3.7. Optimization of CL sensing conditions

In order to obtain the maximum CL signals for propose of obtaining the maximum possible sensitivity of the system, the CL conditions were optimized, as shown in Fig. 8.

The pump speed could have an influence on the degree of mixing of solution, which could affect the stability of CL process. The main pump speed was 30 r/min, and the vice pump speed was 40 r/min. The concentration of NaOH, H_2O_2 and HKUST-1 could directly affect the CL intensity. The optimal concentration of NaOH, H_2O_2 and HKUST-1 were 0.1 mol/L, 0.8 mol/L and 0.05 mg/mL, respectively.

Table 1
Comparing results with different sensor.

Methods	Liner range (mol/L)	Detection limit (mol/L)
HCR [52]	1.0×10^{-6}–1.2×10^{-4}	2×10^{-7}
Fluorescence [63]	3×10^{-10}–1.67×10^{-8}	2.17×10^{-10}
Fluorescence [64]	1.0×10^{-8}–1.0×10^{-7}	5.61×10^{-9}
TRL [65]	–	6×10^{-5}
SERS [66]	5×10^{-9}–5×10^{-7}	5×10^{-9}
This work	1.0×10^{-12}–2.2×10^{-10}	2.1×10^{-13}

3.8. The analytical performance of the CL sensor

For evaluating the applicability of the HKUST-1-based CL sensing system for adenosine, the linear response range and limit of detection (LOD) were measured under the above-mentioned optimum experimental conditions. As shown in Fig. 9, the CL intensity of QDs-luminol-aptamer complex-NaOH-H_2O_2-HKUST-1 system increases obviously with the concentration of adenosine. As shown in Fig. 9, there is a good linear correlation between the CL intensity (I) and the natural logarithm of H_2O_2 concentration (C_{H2O2}) in the range from 1.0×10^{-12} mol/L to 2.2×10^{-10} mol/L with the following equation:

$$\Delta I = 36.3176 \ln c + 1863.1016, (R^2 = 0.9975) \quad (4)$$

The LOD of adenosine was measured to be 2.1×10^{-13} mol/L. This is a good result for the detection of adenosine in the alkaline condition.

In order to make a comprehensive evaluation of the advantages of the presently developed sensor, we compared the performances between the adenosine sensor in this work and other sensors (Table 1). It can be known from the comparison that the linear response range of present adenosine sensor is excellent among adenosine sensor, and the LOD of the presently developed adenosine sensor based on HKUST-1 and QDs-luminol-aptamer conjugates can be well matched with most of the recently reported adenosine sensors based on various solid mimic peroxidases.

3.9. Selectivity of the sensing system

Before applied in real sample detection, selectivity also is an important performance which must be taken into account. The interferences of some coexisted substances in the adenosine standard solution was analyzed under the optimal conditions. While the tolerable limits of coexisting species were taken as a relative error no larger than

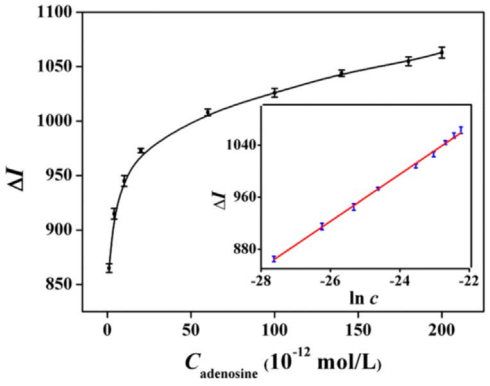

Fig. 9. Relationship between CL intensity (ΔI) and concentration of adenosine.

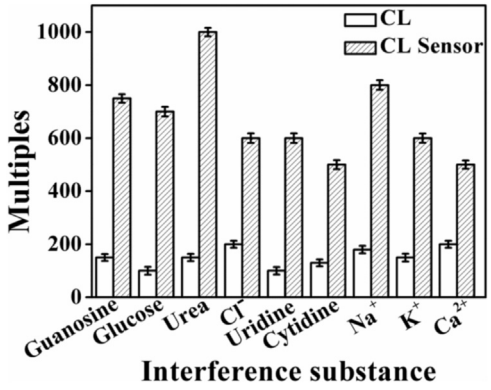

Fig. 10. Interference study of CL sensor.

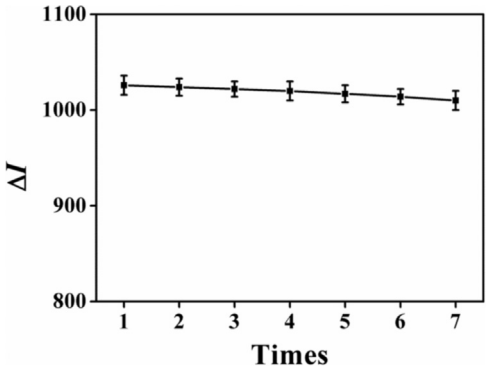

Fig. 11. Reversibility and recyclability of the CL sensor.

Table 2
Application of CL sensor.

Samples	Content (10^{-12} mol/L)	Found (10^{-12} mol/L)	RSD (%)	Recovery (%)
Urine 1#	2.81	3.16	1.3	99
Urine 2#	2.75	2.52	1.4	101.8
Urine 3#	2.27	2.02	2.0	99

5%, the results were shown in Fig. 10.

According to the People's Republic of China Pharmaceutical Industry Standard (YY/T 0475-2011), the consistency of the test results of urine dry chemical analysis method should not be less than 90%, the difference between parallel test results does not exceed one order of magnitude, and the interfering substance concentration does not affect the test results. The experiments show that our sensor could meet the requirements. The experimental results are more reliable.

3.10. Reversibility and recyclability of the CL sensor

When the test was completed, the reversibility and recyclability of the sensor were explored. The waste liquid was collected, and Ni^{2+} was added to the mixed solution to elute adenosine. The mixed solution was centrifuged and the resulting precipitation mixture (containing QDs-luminol-aptamer conjugates and HKUST-1) was dispersed in the MGO solution. Under the action of magnetic field, the supernatant (containing HKUST-1) was separated and adenosine was added to the MGO dispersion. Then, chemiluminescence value of the system was monitored. As shown in Fig. 11., the chemiluminescence intensity decreased from 1026 to 1010 after repeating the above steps 7 times. There was 1.6% chemiluminescence intensity loss in 7 times. It manifested that the CL sensor possessed good reversibility and repeatability, and QDs-luminol-aptamer conjugates and HKUST-1 were very apposite in the biosensor.

3.11. Application of the CL sensor

On the basis of the outstanding characteristics of the proposed method, the feasibility of the CL sensor for adenosine detection was investigated in the work. The CL sensor was applied in human urine samples. As shown in Table 2, the recoveries ranged from 99.0% to 101.8% under optimal experimental conditions. All the above results strongly revealed the capability in urine samples with high reliability and accuracy.

4. Conclusion

In summary, HKUST-1, MGO and QDs-luminol-aptamer conjugates were synthesized for CL detection of adenosine in the alkaline condition. The QDs-luminol-aptamer conjugates can be adsorbed by MGO through π-π conjugation, no CL signal was generated. When adenosine was added, the conjugates were fell off the MGO and the CL switch was turned on. The synthesized QDs-luminol-aptamer conjugates not only to avoid the oxidation of H_2O_2 but also enhanced the CRET efficiency. The obtained HKUST-1 promoted the decomposition of H_2O_2 and improved the sensitivity of the method. The QDs-luminol-aptamer conjugates and HKUST-1 have been used to develop a practical sensor for the detection of adenosine with a wide response range (1.0×10^{-12}–2.2×10^{-10} mol/L) and a low LOD of 2.1×10^{-13} mol/L. It is envisioned that the combination of the different fields of MOFs and CL would be widely used in sensing target analytes in the future.

Acknowledgements

This work was supported by the Shandong Provincial Natural Science Foundation of China (No. ZR2016BM01), and Horizontal Scientific Research Project of China (No. W15077).

References

[1] Suresh K. Srivastava, Vinod K. Gupta, Suresh Jain, PVC-based 2,2,2-cryptand sensor for zinc ions, Anal. Chem. 68 (1996) 1272–1275.
[2] V.K. Gupta, A.K. Singh, M. Al Khayat, Barkha Gupta, Neutral carriers based polymeric membrane electrodes for selective determination of mercury(II), Anal. Chim. Acta 590 (2007) 81–90.
[3] Vinod K. Guptu, Suresh Juin, Upendru Khuranu, A PVC-based pentathia-15-crown-5 membrane potentiometric sensor for mercury(II), Electroanalysis 9 (1997) 478–480.
[4] Vinod Kumar Gupta, S. Kumar, R. Singh, L.P. Singh, S.K. Shoora, B. Sethi, Cadmium (II) ion sensing through p-tert-butyl calix[6]arene based potentiometric sensor, J. Mol. Liq. 195 (2014) 65–68.
[5] Vinod Kumar Gupta, B. Sethi, R.A. Sharma, Shilpi Agarwal, Arvind Bharti, Mercury selective potentiometric sensor based on low rim functionalized thiacalix [4]-arene as a cationic receptor, J. Mol. Liq. 177 (2013) 114–118.
[6] Bradford D. Pendley, Erno Lindner, Medical sensors for the diagnosis and management of disease: the physician perspective, ACS Sens. 2 (2017) 1549–1552.
[7] Rajendra N. Goyal, Vinod K. Gupta, Neeta Bachheti, Fullerene-C_{60}-modified electrode as a sensitive voltammetric sensor for detection of nandrolone-An anabolic steroid used in doping, Anal. Chim. Acta 597 (2007) 82–89.
[8] Vinod Kumar Gupta, Naveen Mergu, Lokesh Kumar Kumawat, Ashok Kumar Singh, Selective naked-eye detection of Magnesium(II) ions using a coumarin-derived fluorescent probe, Sens. Actuators B: Chem. 207 (2015) 216–223.
[9] Vinod Kumar Gupta, Ashok Kumar Singh, Lokesh Kumar Kumawat, Thiazole Schiff base turn-on fluorescent chemosensor for Al^{3+} ion, Sens. Actuators B: Chem. 195 (2014) 98–108.
[10] Eric C. Nallon, Vincent P. Schnee, Collin Bright, Michael P. Polcha, Qiliang Li, Chemical discrimination with an unmodified graphene chemical sensor, ACS Sens. 1 (2016) 26–31.
[11] Kai Jiang, Hongran Zhao, Jianxun Dai, Da Kuang, Teng Fei, Tong Zhang, Excellent humidity sensor based on LiCl loaded hierarchically porous polymeric microspheres, ACS Appl. Mater. Interfaces 8 (2016) 25529–25534.
[12] Vinod Kumar Gupta, L.P. Singh, Rakesh Singh, N. Upadhyay, S.P. Kaur, Bhavana Sethi, A novel copper(II) selective sensor based on Dimethyl 4,4′(o-phenylene) bis(3-thioallophanate) in PVC matrix, J. Mol. Liq. 174 (2012) 11–16.
[13] V.K. Gupta, A.K. Jain, G. Maheshwari, Heinrich Lang, Z. Ishtaiwi, Copper(II)-selective potentiometric sensors based on porphyrins in PVC matrix, Sens. Actuators B: Chem. 117 (2006) 99–106.
[14] V.K. Gupta, A.K. Jain, Pankaj Kumar, PVC-based membranes of N,N′-dibenzyl-1,4,10,13-tetraoxa-7,16-diazacyclooctadecane as Pb(II)-selective sensor, Sens. Actuators B: Chem. 120 (2006) 259–265.
[15] V.K. Gupta, A.K. Jain, P. Kumar, S. Agarwal, G. Maheshwari, Chromium(III)-selective sensor based on tri-*o*-thymotide in PVC matrix, Sens. Actuators B: Chem. 113 (2006) 182–186.
[16] Vinod Kumar Gupta, Naveen Mergu, Lokesh Kumar Kumawat, Ashok Kumar Singh, A reversible fluorescence "off-on-off" sensor for sequential detection of aluminum and acetate/fluoride ions, Talanta 144 (2015) 80–89.
[17] Rajeev Jain, Vinod K. Gupta, N. Jadon, K. Radhapyari, Voltammetric determination of cefixime in pharmaceuticals and biological fluids, Anal. Biochem. 407 (2010) 79–88.
[18] Yuezhen He, Jian Sun, Xiaoxun Wang, Lun Wang, Detection of human leptin in serum using chemiluminescence immunosensor: signal amplification by hemin/G-quadruplex DNAzymes and protein carriers by Fe_3O_4/polydopamine/Au nanocomposites, Sens. Actuators B: Chem. 221 (2015) 792–798.
[19] Haili Yu, Yi He, Wenhao Li, Tao Duan, Graphitic carbon nitride nanosheets-enhanced chemiluminescence of luminol for sensitive detection of 2,4,6-trinitrotoluene, Sens. Actuators B: Chem. 220 (2015) 516–521.
[20] Xiangyi Huang, Jicun Ren, Nanomaterial-based chemiluminescence resonance energy transfer: a strategy to develop new analytical methods, Trends Anal. Chem. 40 (2012) 77–89.
[21] Ji Yang, Zheng-Zhong Lin, Hui-Ping Zhong, Xiao-Mei Chen, Zhi-Yong Huang,

Determination of leucomalachite green in fish using a novel MIP-coated QDs probe based on synchronous fluorescence quenching effect, Sens. Actuators B: Chem. 252 (2017) 561–567.
[22] Tingting Gong, Junfeng Liu, Yiwei Wua, Yao Xiao, Xuehan Wang, Siqi Yuan, Fluorescence enhancement of CdTe quantum dots by HBcAb-HRP for sensitive detection of H_2O_2 in human serum, Biosens. Bioelectron. 92 (2017) 16–20.
[23] Sifang Lv, Feng Chen, Chunyan Chen, Xiaoming Chen, Hang Gong, Changqun Cai, A novel CdTe quantum dots probe amplified resonance light scattering signals to detect microRNA-122, Talanta 165 (2017) 659–663.
[24] Zhao Sheng Qian, Xiao Yue Shan, Lu. Jing Chai, Jian Rong Chen, Hui Feng, A fluorescent nanosensor based on graphene quantum dots-aptamer probe and graphene oxide platform for detection of lead (II) ion, Biosens. Bioelectron. 68 (2015) 225–231.
[25] Hui Chen, Ling Lin, Zhen Lin, Guangsheng Guo, Jin-Ming Lin, Chemiluminescence arising from the decomposition of peroxymonocarbonate and enhanced by CdTe quantum dots, J. Phys. Chem. A 114 (2010) 10049–10058.
[26] Jipei Yuan, Weiwei Guo, Erkang Wang, Quantum dots-bienzyme hybrid system for the sensitive determination of glucose, Biosens. Bioelectron. 23 (2008) 1567–1571.
[27] Zheng Li, Yongxian Wang, Guoxin Zhang, Wanbang Xu, Yanjiang Han, Chemiluminescence resonance energy transfer in the luminol-CdTe quantum dots conjugates, J. Lumin. 130 (2010) 995–999.
[28] Huimin Duan, Leilei Li, Xiaojiao Wang, Yanhui Wang, Jianbo Li, Chuannan Luo, CdTe quantum dots@luminol as signal amplification system for chrysoidine with chemiluminescence-chitosan/graphene oxide-magnetite-molecularly imprinting sensor, Spectrochim. Acta Part A: Mol. Biomol. Spectrosc. 153 (2016) 535–541.
[29] Luc Alaerts, Etienne S5guin, Hilde Poelman, Frédéric Thibault-Starzyk, Pierre A. Jacobs, Dirk E. De Vos, Probing the lewis acidity and catalytic activity of the metal–organic framework $[Cu_3(btc)_2]$ (BTC = Benzene-1,3,5-tricarboxylate), Chem. Eur. J. 12 (2006) 7353–7363.
[30] Fenqiang Luo, Yaolin Lin, Liyan Zheng, Xiaomei Lin, Yuwu Chi, Encapsulation of hemin in metal-organic frameworks for catalyzing the chemiluminescence reaction of the H_2O_2-luminol system and detecting glucose in the neutral condition, ACS Appl. Mater. Interfaces 7 (2015) 11322–11329.
[31] Qian Zhu, Yonglei Chen, Weifeng Wang, Huige Zhang, Cuiling Rena, Hongli Chen, Xingguo Chen, A sensitive biosensor for dopamine determination based on the unique catalytic chemiluminescence of metal-organic framework HKUST-1, Sens. Actuators B: Chem. 210 (2015) 500–507.
[32] Pinghua Ling, Jianping Lei, Lei Zhang, Huangxian Ju, Porphyrin-Encapsulated metal-organic frameworks as mimetic catalysts for electrochemical dna sensing via allosteric switch of hairpin DNA, Anal. Chem. 87 (2015) 3957–3963.
[33] Yali Liu, Wenliang Fu, Chunmei Li, Chengzhi Huang, Yuanfang Li, Gold nanoparticles immobilized on metal-organic frameworks with enhanced catalytic performance for DNA detection, Anal. Chim. Acta 861 (2015) 55–61.
[34] Pinghua Ling, Jianping Lei, Huangxian Ju, Porphyrinic metal-organic framework as electrochemical probe for DNA sensing via triple-helix molecular switch, Biosens. Bioelectron. 71 (2015) 373–379.
[35] Zhongwei Jiang, Pengfei Gao, Lin Yang, Chengzhi Huang, Yuanfang Li, Facile in situ synthesis of silver nanoparticles on the surface of metal-organic framework for ultrasensitive surface-enhanced raman scattering detection of dopamine, Anal. Chem. 87 (2015) 12177–12182.
[36] Ting Lu, Lichun Zhang, Mingxia Sun, Dongyan Deng, Yingying Su, Yi Lv, Amino-functionalized metal-organic frameworks nanoplates-based energy transfer probe for highly selective fluorescence detection of free chlorine, Anal. Chem. 88 (2016) 3413–3420.
[37] Meng Chen, Ning Gan, You Zhou, Tianhua Li, Qing Xu, Yuting Cao, Yinji Chen, A novel aptamer - metal ions - nanoscale MOF based electrochemical biocodes for multiple antibiotics detection and signal amplification, Sens. Actuators B: Chem. 242 (2017) 1201–1209.
[38] Tiziana Musso, Priyank V. Kumar, Adam S. Foster, Jeffrey C. Grossman, Graphene oxide as a promising hole injection layer for MoS_2-based electronic devices, ACS Nano 8 (2014) 11432–11439.
[39] Hamed Dalir, Yang Xia, Yuan Wang, Xiang Zhang, Athermal broadband graphene optical modulator with 35 GHz speed, ACS Photon. 3 (2016) 1564–1568.
[40] Esmaiel Nouri, Yu-Long Wang, Qian Chen, Jia-Ju Xu, Georgios Paterakis, Vassilios Dracopoulos, Zong-Xiang Xu, Dimitrios Tasis, Mohammad Reza Mohammadi, Panagiotis Lianos, Introduction of graphene oxide as buffer layer in perovskite solar cells and the promotion of soluble n-Butyl-substituted copper phthalocyanine as efficient hole transporting material, Electrochim. Acta 233 (2017) 36–43.
[41] Hong Yuan, Jia Liu, Qingze Jiao, Yongjian Li, Xiufeng Liu, Daxin Shi, Qin Wu, Yun Zhao, Hansheng Li, Sandwich-like octahedral cobalt disulfide/reduced graphene oxide as an efficient Pt-free electrocatalyst for high-performance dye-sensitized solar cells, Carbon 119 (2017) 225–234.
[42] Jun-Seok Yeo, Cheol-Ho Lee, Dawon Jang, Sungho Lee, Seung Mu Jo, Han-Ik Joh, Dong-Yu Kim, Reduced graphene oxide-assisted crystallization of perovskite via solution-process for efficient and stable planar solar cells with module-scales, Nano Energy 30 (2016) 667–676.
[43] Mathieu Saulnier, Charles Trudeau, Sylvain G. Cloutier, Steen B. Schougaard, Investigation of CVD multilayered graphene as negative electrode for lithium-ion batteries, Electrochim. Acta 244 (2017) 54–60.
[44] Elmar Yu Kataev, Daniil M. Itkis, Alexander V. Fedorov, Boris V. Senkovsky, Dmitry Yu Usachov, Nikolay I. Verbitskiy, Alexander Grüneis, Alexei Barinov, Daria Yu Tsukanova, Andrey A. Volykhov, Kirill V. Mironovich, Victor A. Krivchenko, Maksim G. Rybin, Elena D. Obraztsova, Clemens Laubschat, Denis V. Vyalikh, Lada V. Yashina, Oxygen reduction by lithiated graphene and graphene-based materials, ACS Nano 9 (2015) 320–326.
[45] Onur Parlak, Anthony P.F. Turner, Ashutosh Tiwari, On/off-switchable zipper-like bioelectronics on a graphene interface, Adv. Mater. 26 (2014) 482–486.
[46] Fei Qu, Dongya Liu, Jinmao You, Fluorescent turn-off/on bioassay for hemoglobin based on dual-emission carbon nanodots-graphene oxide system with multi-detection strategies, Anal. Chim. Acta 921 (2016) 59–66.
[47] Xionghui Ma, Jianping Li, Yunbin Liu, Yali Yuan, Guobao Xu, Construction of a Concanavalin A electrochemical sensor base on a novel sandwich capture mode, Sens. Actuators B: Chem. 248 (2017) 201–206.
[48] Hyuk Joon Kim, Seul-Yi Lee, Le. Hoang Sinh, Chang Su Yeo, Yeong Rae Son, Kang Rae Cho, YoonKyu Song, Sanghyun Ju, Min Kyoon Shin, Soo-Jin Park, SangYoon Park, Maximizing volumetric energy density of all-graphene-oxide-supercapacitors and their potential applications for energy harvest, J. Power Sources 346 (2017) 113–119.
[49] Lin Zhang, Hongchang Yao, Zhaohui Li, Piaopiao Sun, Fei Liu, Cui Dong, Jianshe Wang, Zhongjun Li, Mingwei Wu, Chang Zhang, Bo Zhao, Synthesis of delaminated layered double hydroxides and their assembly with graphene oxide for supercapacitor application, J. Alloy. Compd. 711 (2017) 31–41.
[50] Hua Zhou, Bin Gao, Yanmei Zhou, Han Qiao, Wenli Gao, Haonan Qu, Shanhu Liu, Qingyou Zhang, Xiaoqiang Liu, Facile preparation of 3D GO/CNCs composite with adsorption performance towards [BMIM][Cl] from aqueous solution, J. Hazard. Mater. 337 (2017) 27–33.
[51] Michelle Mujoomdar, David Hoskinb, Jonathan Blay, Adenosine stimulation of the proliferation of colorectal carcinoma cell lines Roles of cell density and adenosine metabolism, Biochem. Pharmacol. 66 (2003) 1737–1747.
[52] Chunjing Feng, Zhun Hou, Wei Jiang, Lihong Sang, Lei Wang, Binding induced colocalization activated hybridization chain reaction on the surface of magnetic nanobead for sensitive detection of adenosine, Biosens. Bioelectron. 86 (2016) 966–970.
[53] Dan Wu, Xiang Ren, Lihua Hu, Dawei Fan, Yang Zheng, Qin Wei, Electrochemical aptasensor for the detection of adenosine by using PdCu@MWCNTs-supported bi-enzymes as labels, Biosens. Bioelectron. 74 (2015) 391–397.
[54] Jing Shen, Hongyang Wang, Chunxiang Li, Yanyan Zhao, Xijuan Yu, Xiliang Luo, Label-free electrochemical aptasensor for adenosine detection based on cascade signal amplification strategy, Biosens. Bioelectron. 90 (2017) 356–362.
[55] Jiewei Sun, Wei Jiang, Jing Zhu, Wei Li, Lei Wang, Label-free fluorescence dual-amplified detection of adenosine based on exonuclease III-assisted DNA cycling and hybridization chain reaction, Biosens. Bioelectron. 70 (2015) 15–20.
[56] Xiluan Yan, Zhijuan Cao, Masaaki Kai, Jianzhong Lu, Label-free aptamer-based chemiluminescence detection of adenosine, Talanta 79 (2009) 383–387.
[57] Lei Xu, Xin Shen, Bingzhi Li, Chunhong Zhu, Xuemin Zhou, G-quadruplex based Exo III-assisted signal amplification aptasensor for the colorimetric detection of adenosine, Anal. Chim. Acta 980 (2017) 58–64.
[58] Benoit Chovelon, Guillaume Durand, Eric Dausse, Jean-Jacques Toulme, Patrice Faure, Eric Peyrin, Corinne ravelet, ELAKCA: enzyme-linked aptamer kissing complex assay as a small molecule sensing platform, Anal. Chem. 88 (2016) 2570–2575.
[59] Peng Hu, Chengzhou Zhu, Lihua Jin, Shaojun Dong, An ultrasensitive fluorescent aptasensor for adenosine detection based onexonuclease III assisted signal amplification, Biosens. Bioelectron. 34 (2012) 83–87.
[60] W.S. Hummers Jr., R.E. Offeman, Preparation of graphitic oxide, J. Am. Chem. Soc. 80 (1958) (1339-1339).
[61] M.Z. Kassaee, E. Motamedi, M. Majdi, Magnetic Fe_3O_4-graphene oxide/polystyrene: fabrication and characterization of a promising nanocomposite, Chem. Eng. J. 172 (2011) 540–549.
[62] S.S.-Y. Chui, S.M.-F. Lo, J.P.H. Charmant, A.G. Orpen, I.D. Williams, A chemically functionalizable nanoporous material $[Cu_3(TMA)_2(H_2O)_3]_n$, Science 283 (1999) 1148–1150.
[63] Yueyue Song, Tang Tang, Xu Wang, Guanhong Xu, Fangdi Wei, Yanzi Wu, Quan Song, Yujie Ma, Yunsu Ma, Yao Cen, Qin Hu, Highly selective and sensitive detection of adenosine utilizing signal amplification based on silver ions-assisted cation exchange reaction with CdTe quantum dots, Sens. Actuators B: Chem. 247 (2017) 305–311.
[64] Da-Wei Huang, Cheng-Gang Niu, Guang-Ming Zeng, Min Ruan, Time-resolved fluorescence biosensor for adenosine detection based on home-made europium complexes, Biosens. Bioelectron. 29 (2011) 178–183.
[65] Le-Le Li, Pinghua Ge, Paul R. Selvin, Yi Lu, Direct detection of adenosine in undiluted serum using a luminescent aptamer sensor attached to a terbium complex, Anal. Chem. 84 (2012) 7852–7856.
[66] Shicai Xu, Baoyuan Man, Shouzhen Jiang, Jihua Wang, Jie Wei, Shida Xu, Hanping Liu, Shoubao Gao, Huilan Liu, Zhenhua Li, Hongsheng Li, Hengwei Qiu, Graphene/Cu nanoparticle hybrids fabricated by chemical vapor deposition as surface-enhanced raman scattering substrate for label-free detection of adenosine, ACS Appl. Mater. Interfaces 7 (2015) 10977–10987.